Multiplatform observations of boundary layer structure in the outer rainbands of landfalling typhoons

Jie Ming and Yuan Wang

Key Laboratory of Mesoscale Severe Weather, Ministry of Education, School of Atmospheric Sciences, Nanjing University, Nanjing, China

1. Introduction

It has long been recognized that the boundary layer (BL) plays an important role in the development and maintenance of tropical cyclones (TCs), because TCs interact with the ocean/land through the BL, exchanging momentum, heat and moisture. As part of an experiment supported by the National Key Basic Research and Development Program of China (973 program), a new observational network was set up on the eastern coast of China. It consists of a mobile observing system (referred to as MOS hereafter), meteorological tower, automatic weather station, and Doppler radars. These data allow scientists to study the BL structures in landfalling TCs. The objective of this paper is to provide an example of how these observations can be used to document the structure and evolution of the BL during TC landfall. In the case shown here, we will identify the kinematic and thermodynamic differences of the BL during and after convection during the landfall of Typhoon Morakot (2009). It is the first time that the data from the MOS and towers have been used together, which allows us to study the evolution of both the mean and turbulent structure in the BL of the outer core region during convective and post-convective periods. We aim to analyze the physical processes in the BL and their interaction with TC convection using the data from the new observing platform and give an explanation of the evolution of the BL. We hope that these results can provide useful information for evaluating and improving the PBL schemes in TC models.

2. Data description

- The data used in this paper were collected by multiple radars, automatic weather stations, one MOS and one meteorological tower during Typhoon Morakot's landfall in southeast China.
- Summary of the instrumentation used in this study with deployment locations, observed variables and time periods of observation.

Instruments	Locations	Variables	Time periods
WZRD	27.89 ºN, 120.74 ºE	Radar relectivity (dBZ)	0000 UTC 8 ~1200 UTC 9 August
FZRD	25.98 ºN, 119.53 ºE	Radar relectivity (dBZ)	0000 UTC 8 ~1200 UTC 9 August
XMRD	24.48 ºN, 118.08 ºE	Radar relectivity (dBZ)	0000 UTC 8 ~ 1200 UTC 9 August
AWS1	26.64 ºN, 119.67 ºE	Hourly rainfall (hr mm^{-1})	0000 ~ 1200 UTC 9 August
AWS2	26.67 ºN, 119.52 ºE	Temperature (K), dew point temperature (K) and pressure (hPa)	0000 ~ 1200 UTC 9 August
Ultrasonic anemometer on MOS	26.66 ºN, 119.55 ºE	Three dimensional wind speed on 10-m height (u, v, w, m s^{-1})	0200 ~ 1000 UTC 9 August
GPS system on MOS	26.66 ºN, 119.55 ºE	Temperature (K), dew point temperature (K), pressure (hPa), relative humidity (%), wind speed (m s^{-1}) and wind direction (º)	0227 ~ 0314 UTC, 0533 ~0606 UTC, 0830 ~ 0918 UTC 9 August
Meteorological tower	27.97 ºN, 121.07 ºE	Horizontal wind speed at 10, 30, 50 and 70 m height (m s^{-1}) and wind direction at 10, 50 and 70 m height (º)	0400 ~ 0800 UTC 9 August

3. Analysis method

Figure 1 shows the merged radar reflectivity at the location of the MOS for the period from 0000 UTC to 1000 UTC 9 August. The distance from the MOS to the storm center was between 50 and 150 km. We will categorize the periods based on observed radar reflectivity to investigate the differences in the BL structure between the convective and post-convective periods. Based on the magnitude of radar reflectivity, the post-convective period is defined as the maximum radar reflectivity < 15 dBZ and the convective period is defined as maximum radar reflectivity > 35 dBZ.The three circles in Fig.3 represent the three periods of observation we are interested in. The first circle represents a post-convective period (0200 UTC to 0330 UTC), the second is a convective period (0430 UTC to 0600 UTC), and the third is another post-convective period (0800 UTC to 0930 UTC).

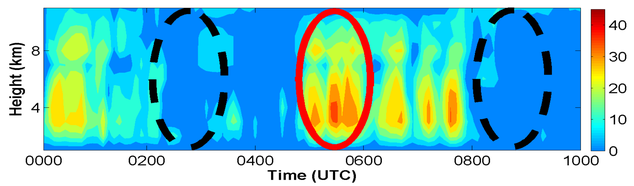

Figure 1 Time-height series of radar reflectivity (dBZ) at the position of MOS from 0000 UTC to 1000 UTC 9 August 2009. Red circle marks the convective period and black dashed circles mark the post-convective periods.

4. Mean boundary layer structure and Turbulence properties

1) Figure 2 shows the comparison of the vertical profiles of theta-v, tangential and radial winds observed by the GPS system for the convective and post-convective periods. Firstly, the estimated mixed layer depth is ~260 m between 0533 - 0606 UTC on 09 August, which is defined as the convective period (Table 2). However the mixed layer is much shallower (~150 m) during the post-convective periods (0227-0314 UTC and 0830-0918 UTC). The maximum tangential winds in the post-convective periods are above 2000 m. During the convective period, the BL height based on h_{vtmax} is approximately 1600 m. The inflow layer depths in these three periods are clearly defined: below 1000 m in two periods post the convection and around 1500 m in the period with convection. Interestingly, the height of the maximum tangential wind speed is found to be above the inflow layer depth for three periods.

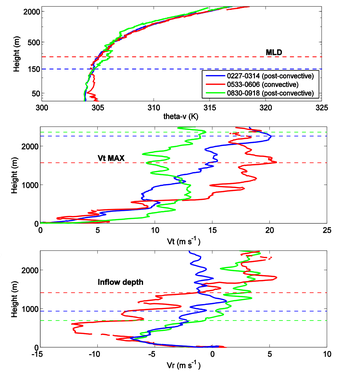

Figure 2 The Vertical profiles of virtual potential temperature (K), tangential wind component (m s^{-1}) and radial wind component (m s^{-1}) during 0227-0314 UTC (blue and dashed line, post-convective period), 0533-0606 UTC (red and solid line, convective period) and 0830-0918 UTC (green and pecked line, post-convective period) 9 August.

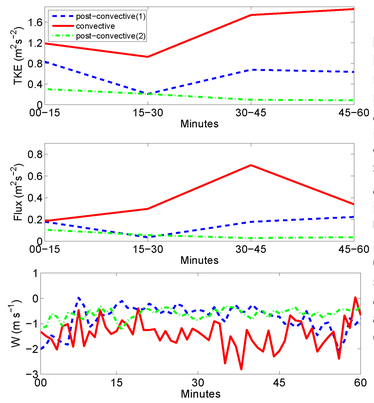

Figure 3 Plots of turbulent kinetic energy (TKE) (unit: m^2 s^{-2}), momentum flux (unit: m^2 s^{-2}) measured by the MOS averaged over 15 minutes increments and 10-m height vertical velocity (unit: m s^{-1})measured by the MOS averaged over 1 minute increments during0227-0314 UTC (blue and dashed line, post-convective period), 0533-0606 UTC (red and solid line, convective period) and 0830-0918 UTC (green and pecked line, post-convective period) 9 August.

2) During the convective period, two strong convective cells are observed with the radar reflectivity greater than 25 dBZ extending to 8~10 km altitude. The maximum value of TKE increased up to 1.8 m^2 s^{-2}, which is much larger than that during the post-convective periods. The maximum 15 min averaged value of momentum flux is below 0.2 m^2 s^{-2}, during the post-convective periods, which is nearly three times larger during the convective period. During the convective period, it appears that the momentum flux increases at the same time that the TKE increases. It also shows that the convective period has much stronger downdrafts than the post-convective periods. There is a strong correlation between the vertical velocity and TKE as well as momentum flux, indicating that penetrating convective downdrafts can reach the surface and enhance turbulent fluxes and mixing.

5. Summary

The schematic diagram shows that the thermodynamic mixed layer is within the inflow layer, consistent with the dropsonde composite analysis result given by Zhang et al. [2011c]. Both the thermodynamic BL height and inflow layer depth are found to be deeper within convective period than during post-convective periods. The height of the maximum tangential wind speed is found to be above the inflow layer for both situations. Furthermore, the tangential and radial wind velocities are larger in the convective period than the post-convective periods. The magnitude of downward motion is also found to be much larger in the convective period than the post-convective periods.

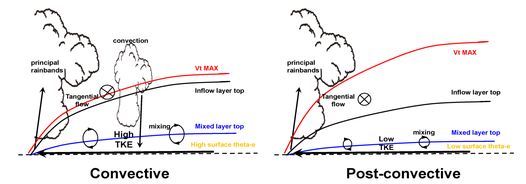

Figure 4 Schematic diagram summarizing the evolution of BL structures during the landfall of Typhoon Morakot (2009) for two periods.

Acknowledgments: **This research is supported by National Key Basic Reaearch and Development Project of China (973: 2009CB421502 and 2013CB430100), the National Natural Science Foundation of China (grants 41105035).**

For further details see the paper:

Ming, J., J. A. Zhang, R. F. Rogers, F. D. Marks, Y. Wang, and N. Cai, 2014: Multiplatform observations of boundary layer structure in the outer rainbands of landfalling typhoons. Journal of Geophysical Research, 119, doi: 10.1002/2014JD021637.